Metabolism 181 (2026) 156636

Contents lists available at ScienceDirect

Metabolism

journal homepage: www.journals.elsevier.com/metabolism

Islet inflammatory macrophages drive MSC loss and multiple interactions involved in β-cell adaptation during diabetes

Jianxing Liu [a,1], Weilong Xu [b,1], Wenjing Yan [a,1], Yimeng Qin [a], Xintong Wang [a], Xiuning Chen [c], Zhaoyou Meng [d], Yi Pan [a], Yanfeng Zhang [a], Yumeng Shen [a], Yue Yang [a], Fangfang Zhang [a], Hailiang Liu [e], Pengfei Zheng [c,*,2], Jiangyi Yu [b,**,2], Liang Jin [a,***,2]

[a] State Key Laboratory of Natural Medicines, Jiangsu Key Laboratory of Druggability of Biopharmaceuticals, School of Life Science and Technology, China Pharmaceutical University, 24 Tongjiaxiang, Nanjing, China
[b] Department of Endocrinology, Jiangsu Province Hospital of Chinese Medicine, Affiliated Hospital of Nanjing University of Chinese Medicine, Nanjing, China
[c] Department of Orthopaedic Surgery, Children's Hospital of Nanjing Medical University, Nanjing, Jiangsu, China.
[d] Department of Neurology, Second Affiliated Hospital of Army Medical University, Chongqing, China
[e] Institute for Regenerative Medicine, Shanghai East Hospital, Tongji University School of Medicine, Shanghai, 200123, China

ARTICLE INFO

Keywords:
Diabetes
Mesenchymal stem cell
β-cells adaptation
Macrophage

ABSTRACT

While the functional adaptation of β-cells during type 2 diabetes progression is well-established, the role of non-β islet cells remains largely unexplored. Utilizing single-cell RNA sequencing, we identified a substantial expansion of the macrophage population and a concomitant reduction in the proportion of mesenchymal stem cells (MSCs) within the islets of diabetic mice transitioning from metabolic compensation to decompensation. Under conditions of metabolic stress, macrophages extensively infiltrated the islets and adopted a pronounced pro-inflammatory phenotype. This phenotypic shift impaired β-cell glucose-stimulated insulin secretion and induced β-cell apoptosis. Simultaneously, macrophage-derived inflammatory factors, notably TNF-α, suppressed MSC proliferation and downregulated Wntless (Wls), thereby reducing extracellular Wnt transport. The resultant loss of Wls diminished MSCs' capacity to provide trophic support to β-cells and hindered the transition of macrophages to an anti-inflammatory phenotype. This self-perpetuating cycle establishes a chronic pro-inflammatory environment within the islets, culminating in β-cell functional deterioration and the onset of diabetes. Experimental intervention involving macrophage elimination and MSC administration was shown to disrupt this detrimental cycle, restoring β-cell function and glycemic control. Collectively, our findings reveal that macrophages and MSCs jointly govern β-cell adaptation through intricate paracrine crosstalk. Modulating these macrophage-MSC interactions holds significant therapeutic implications for maintaining β-cell integrity and underscores the considerable potential of MSC-based therapies for type 2 diabetes treatment.

1. Introduction

Obesity is a well-recognized risk factor for developing type 2 diabetes mellitus (T2DM). However, it is important to note that not all obese individuals develop diabetes, as some can maintain relatively stable blood glucose levels by appropriately increasing their blood insulin levels [1,2]. Nevertheless, a progressive decline in compensatory β-cell proliferation and insulin secretion ultimately renders insulin inadequate to counteract insulin resistance, prompting the transition from compensation to decompensation [3–5]. The adaptation of β-cell function is a core process in the onset of diabetes [6,7]. Nevertheless, the mechanisms and signaling that underlie β-cell compensation and

* Corresponding author.
** Correspondence to: J. Yu, Department of Endocrinology, Jiangsu Province Hospital of Chinese Medicine, Affiliated Hospital of Nanjing University of Chinese Medicine, Nanjing, China.
*** Correspondence to: L. Jin, State Key Laboratory of Natural Medicines, Jiangsu Key Laboratory of Druggability of Biopharmaceuticals, School of Life Science and Technology, China Pharmaceutical University, 24 Tongjiaxiang, Nanjing, China.
E-mail addresses: zhengpengfei@njmu.edu.cn (P. Zheng), yjy202105@njucm.edu.cn (J. Yu), ljstemcell@cpu.edu.cn (L. Jin).
[1] Co-first author.
[2] Co-senior authors.

https://doi.org/10.1016/j.metabol.2026.156636
Received 8 October 2025; Accepted 13 May 2026
Available online 16 May 2026

subsequent decompensation remain unclear.

Recent research highlights the dynamic influence of the islet microenvironment on pancreatic β-cell functional integrity, with non-β islet cells playing a crucial regulatory role [8,9]. Infiltrating immune cells, particularly macrophages, orchestrate islet inflammation during obesity [8,10]. Internal islet macrophages sense metabolic stress and inflammation, regulating β-cell proliferation and function [11,12]. However, infiltrating macrophages can negatively affect β-cell functional adaptation [11,13].

Tissue often preserves cells that maintain tissue homeostasis, such as mesenchymal stem cells (MSCs). These cells are found in nearly all tissues and are essential for tissue repair and inflammatory regulation [14–16]. In diabetic conditions, the administration of MSCs enhances β-cell regeneration and supports the function and viability of transplanted islets in vivo [17–19]. Animal models and clinical studies show that MSC administration improves glycemic control and reduces insulin resistance in diabetes by suppressing macrophage inflammation [19–21]. However, it remains uncertain whether MSCs interact with macrophages and play a role in the adaptation of β-cells as diabetes progresses.

In this study, we used a T2DM mouse model fed a high-fat diet (HFD) to investigate the effects of non-β islet cells on β-cell function and conversion. Our findings demonstrate that infiltrating islet macrophages reduce MSC abundance and secretory capacity, compromising trophic support for β-cell proliferation and insulin secretion, and weakening the inflammatory regulation of macrophages. The interplay between MSCs and macrophages participate in the β-cell functional adaptation and the conversion of T2DM from compensation to decompensation.

2. Methods

2.1. Animal models

Male C57BL/6J and C57BL/6-Tg (ACTB-EGFP)1Osb/J mice were purchased from Hangzhou Ziyuan Experimental Animal Technology Co., Ltd. [SCXK (Zhe) 2019-0004]. The mice were housed in groups of 3–5 animals per cage under a 12-hour light-dark cycle in an SPF-grade animal facility, with ambient temperature maintained at 22–24 °C and relative humidity at 40–50%. All animals had ad libitum access to standard laboratory chow and drinking water. All animal experiments were conducted in accordance with the national guidelines for laboratory animal care and use, and were approved by the Institutional Animal Care and Use Committee of China Pharmaceutical University (Nanjing, China; Permit No. 2162326).

To establish a diet-induced obesity model and mimic the progression from compensated to decompensated diabetic status, 10-week-old male C57BL/6J mice were fed either a high-fat diet (HFD, 60 kcal% fat, D12492, Research Diets) or a normal chow diet (10 kcal% fat, D12450J, Research Diets).

2.2. IPGTT and IPITT

IPGTT and IPITT were performed as previously described [22]. For the IPGTT, mice were fasted for 16 h and intraperitoneally injected with glucose solution at a dose of 1.2 g/kg body weight. For the IPITT, mice were fasted for 8 h and intraperitoneally injected with insulin solution at a dose of 0.5 U/kg body weight. Blood glucose levels were measured from tail vein blood at 0, 15, 30, 60, 90, and 120 min following glucose or insulin administration.

2.3. Primary islet isolation and scRNA sequencing

Islets were isolated via enzymatic digestion as described in our previous study [23]. Single-cell library preparation was carried out following a previously reported protocol [24]. Briefly, single cells (approximately 2.0×10^5 cells) isolated from an equivalent of 200 islets of mice fed a high-fat diet for 9 or 15 weeks were prepared for scRNA-seq. Library sequencing was performed on the Illumina NextSeq 500 platform at the Institute for Regenerative Medicine, Shanghai East Hospital. Cells were filtered according to the following quality control criteria: (i) genes detected in at least 10 cells; (ii) nCount-RNA ranging from 200 to 4000; (iii) mitochondrial gene content below 10%. Raw data were normalized and batch-corrected using Harmony, followed by cell clustering with UMAP. Cell types were annotated based on canonical marker genes: *Ins1* (*β*-cell), *Gcg* (α-cell), *Sst* (δ-cell), *Ppy* (pp-cell), *Rgs5* (myofibroblast), *Reg1* (glandular EC), *CD73* and *Stmn1* (MSC), *CD74* (macrophage), *Dcn* (fibroblast), *Krt19* (ductal cell), and *Flt1* (capillary venous EC). Differential gene expression analysis was performed using the generalized linear mixed model implemented in MAST. Genes with $|\log_2 FC| \geq 1.25$ and $p < 0.05$ were defined as significantly differentially expressed.

2.4. Insulin secretion assay

MIN6 cells and isolated islets (30 islets per well) were cultured in RPMI 1640 medium supplemented with 2.5 mM glucose and 10% FBS for 24 h. After equilibration in KRBH buffer, cells and islets were further incubated with 2.5 mM or 16.7 mM glucose for 2 h. Insulin concentrations in the culture supernatant were measured and normalized to the total protein content of whole-cell lysates.

2.5. Islet area and β-cell mass analysis

The pancreas tissues were dissected, paraffin-embedded, and serially sectioned at 5 μm (6 mice per group). Slides were selected at an interval of 100 μm, with 6 slides collected per mouse. These sections were stained with hematoxylin and eosin (H&E) or processed for insulin immunofluorescence staining, respectively. Islet area was calculated as the ratio of islet area to total pancreatic cross-sectional area, and β-cell mass was determined by multiplying pancreatic weight by the ratio of insulin-positive area to total pancreatic area [25].

2.6. Islet β-cell proliferation and apoptosis

β-cell proliferation was assessed by immunofluorescence co-staining for Ki67 and insulin, as well as by an EdU incorporation assay. β-cell apoptosis was evaluated using TUNEL and insulin double immunofluorescence staining. Paraffin-embedded pancreatic tissues from six mice were serially sectioned at 100 μm intervals and stained for Ki67, TUNEL, and insulin. At least eight islets were quantified per section.

2.7. ELISA assay

The levels of cytokines and insulin in mouse serum and cell culture supernatants were measured using commercial ELISA kits (Jiangsu Boshen Biotechnology Co., Ltd., China).

2.8. Proportion of MSCs in islets

MSCs were identified as the $CD31^-CD45^-CD146^-$ $Vimentin^-CD73^+CD90^+$ cell subset. Islet single cells were co-stained with fluorescently conjugated anti-mouse antibodies (Biolegend) for flow cytometry: PerCP/Cyanine5.5-CD31 (Cat# 102420), FITC-CD45 (Cat# 157213), PE/Cyanine7-CD146 (Cat# 134713), Alexa Fluor 647-Vimentin (Cat# 699307), APC-CD73 (Cat# 127210), and PE-CD90 (Cat# 140307). Cells were subsequently analyzed by flow cytometry using a BD FACS Celesta instrument (Becton Dickinson).

2.9. Islet-derived MSCs culture, identification, and differentiation

Islets were isolated via collagenase digestion and cultured in low-glucose DMEM (L-DMEM) supplemented with 10% FBS for 72 h.

Adherent cells were maintained and passaged by trypsinization. For cell identification, cells were stained with fluorescent-conjugated antibodies: PerCP/Cyanine5.5-CD31, FITC-CD45, APC-CD73, PE-CD29, PE-CD90, PE/Cyanine7-CD146, and Alexa Fluor 647-Vimentin, along with corresponding isotype IgG controls.

Third-passage cells were induced to undergo MSCs multilineage differentiation. For adipogenic differentiation, cells were cultured in high-glucose DMEM (H-DMEM) complete medium containing 0.5 mM IBMX, 0.5 μM dexamethasone, 200 μM indomethacin, and 1 μg/mL insulin. For osteogenic differentiation, cells were cultured in medium supplemented with 10 mM β-glycerophosphate, 0.1 μM dexamethasone, and 50 μg/mL ascorbic acid. For chondrogenic differentiation, cells were cultured in medium containing 0.1 μM dexamethasone, 10 ng/mL TGF-β1, 50 nM ascorbic acid, and 6.25 μg/mL insulin. Adipogenic, osteogenic, and chondrogenic differentiation capacities were evaluated by Oil Red O, Alizarin Red, and Alcian Blue staining, respectively.

2.10. MSCs' secretory capacity assay

MSCs were cultured in serum-free medium for 24 h. Cell culture supernatants were harvested, and total protein concentrations were quantified using the Bicinchoninic Acid (BCA) assay (VAzyme, Cat# E112-01). All results were normalized to the total protein content of whole-cell lysates.

2.11. Proliferation, senescence, and apoptosis assay

Cell proliferation was assessed using an EdU incorporation assay and a colony formation assay. For the colony formation assay, cells were stained with 0.1% crystal violet solution for 30 min. After elution with 10% acetic acid and thorough shaking, absorbance was measured quantitatively at 570 nm. Cell apoptosis was detected via flow cytometry using an Annexin V-FITC/PI apoptosis detection kit (Multi Science, Cat# AP107). Cellular senescence was evaluated with a Senescence β-Galactosidase Staining Kit (Beyotime Institute of Biotechnology, Cat# C0602).

2.12. Cells migration

A total of 2×10^4 cells were seeded into 12-well Transwell inserts (5 μm pore size for macrophages and 12 μm pore size for MSCs) and cultured for 24 h. Cells were stained with 0.1% crystal violet. Migratory cells on the lower surface of the Transwell inserts were counted, and migration ability was normalized to the total number of cells initially seeded in each chamber.

2.13. Proportion and polarization of macrophages in islets

Macrophages were identified using an anti-F4/80 antibody (Biolegend, Cat# 123107). Macrophage polarization was further characterized by staining with PE-CD86 (Biolegend, Cat# 159204) and APC-CD206 (Biolegend, Cat# 141708), with corresponding isotype IgG serving as negative controls. All analyses were performed by flow cytometry.

2.14. Islet macrophage and β-cell enrichment

F4/80-positive cells within pancreatic islets were sorted using a CytoFLEX SRT flow cytometer (BD, San Jose, CA) and cultured in complete L-DMEM. β-cells were isolated based on cellular flavin adenine dinucleotide autofluorescence as previously reported by Heimberg et al. [26]. Briefly, isolated islet single cells were washed with Ham's F-10 medium supplemented with 6 mM glucose, 1% bovine serum albumin, and 2 mM L-glutamine, then incubated in suspension for 30 min. β-cells were subsequently sorted by FACS according to intrinsic flavin adenine dinucleotide autofluorescence, with excitation at 488 nm and emission collected at 510–550 nm (FITC filter) on the CytoFLEX SRT.

2.15. BMDM differentiation and tracking

Bone marrow-derived macrophage (BMDM) suspensions were isolated from the tibias and femurs of hind limbs of C57BL/6-Tg (ACTB-EGFP)1Osb/J mice. Cells were differentiated with 50 ng/mL recombinant mouse M-CSF (Proteintech, Cat# HZ-1192) for 7 days. Differentiated BMDMs were then transferred into recipient mice via intravenous injection at a dose of 2.5×10^5 cells in 0.1 mL. The engraftment of $EGFP^+$ cells within pancreatic islets of recipient mice was examined by flow cytometry and immunofluorescence staining at 24 h after macrophage intravenous injection.

2.16. Cells co-culture

Macrophages (or RAW264.7), β-cells (or MIN6), and MSCs were co-cultured using a Transwell system (Corning, 1.0 μm pore size). For separate co-culture experiments, MSCs were seeded in the lower chamber, with macrophages or β-cells plated in the upper chamber; the reverse setup was also performed (MSCs: macrophages = 1:2; MSCs: β-cells = 1:10).

For multicellular co-culture, 30 isolated islets were cultured in the lower chamber, while MSCs and macrophages were seeded in Transwell inserts (upper chamber) at 80% confluence (MSCs: macrophages = 1:2).

2.17. Dual-luciferase reporter assay

293T cells were co-transfected with pGL3-Luc::Wls together with either IRF3 overexpression plasmid or empty control vector (pcDNA3.1), along with the pGMLR-CMV luciferase reporter. After 48 h, firefly luciferase activity was measured and normalized to Renilla luciferase activity (Vazyme, Cat# DL101-01).

2.18. ROS assay

Intracellular ROS levels in macrophages (or RAW264.7 cells) were assessed. Cells were preincubated with 10 μM DCFH-DA (Beyotime Institute of Biotechnology, Cat# S0033S) for 30 min, followed by analysis using flow cytometry.

2.19. Macrophage cellular energy metabolism

Primary macrophages and RAW264.7 cells (8×10^4 cells per well) were seeded onto Seahorse XF96 V3 PS Cell Culture Microplates and incubated for 8 h. The oxygen consumption rate (OCR) was then measured using an Agilent Seahorse XF96 Bioanalyzer (Agilent, Santa Clara, CA, USA). OCR was assessed under basal conditions and following sequential treatment with 1 μM oligomycin, 1 μM FCCP [carbonyl cyanide 4-(trifluoromethoxy) phenylhydrazone], and 0.5 μM rotenone/antimycin A, according to the manufacturer's instructions.

2.20. Ca^{2+} influx

MIN6 cells and primary β-cells were loaded with 5 μM Fluo-4 AM (Solarbio, Cat# IF1500) in glucose- and Ca^{2+}/Mg^{2+}-free HBSS for 30 min. The Fluo-4 AM solution was then removed, and baseline as well as glucose-stimulated Ca^{2+} influx was recorded at 50 ms intervals using a BioTek Cytation 5 Hybrid Multimode Reader (BioTek, Vermont, USA).

2.21. Mice macrophage depletion

Mice received intraperitoneal injections of either Clophosome-A-Clodronate Liposomes or control liposomes (LIPOSOMA, Cat# F70101C-A) at a dose of 1.4 mg per 20 g body weight, administered twice weekly for two consecutive weeks. Three days after the final injection, macrophage depletion efficiency was verified by flow cytometry.

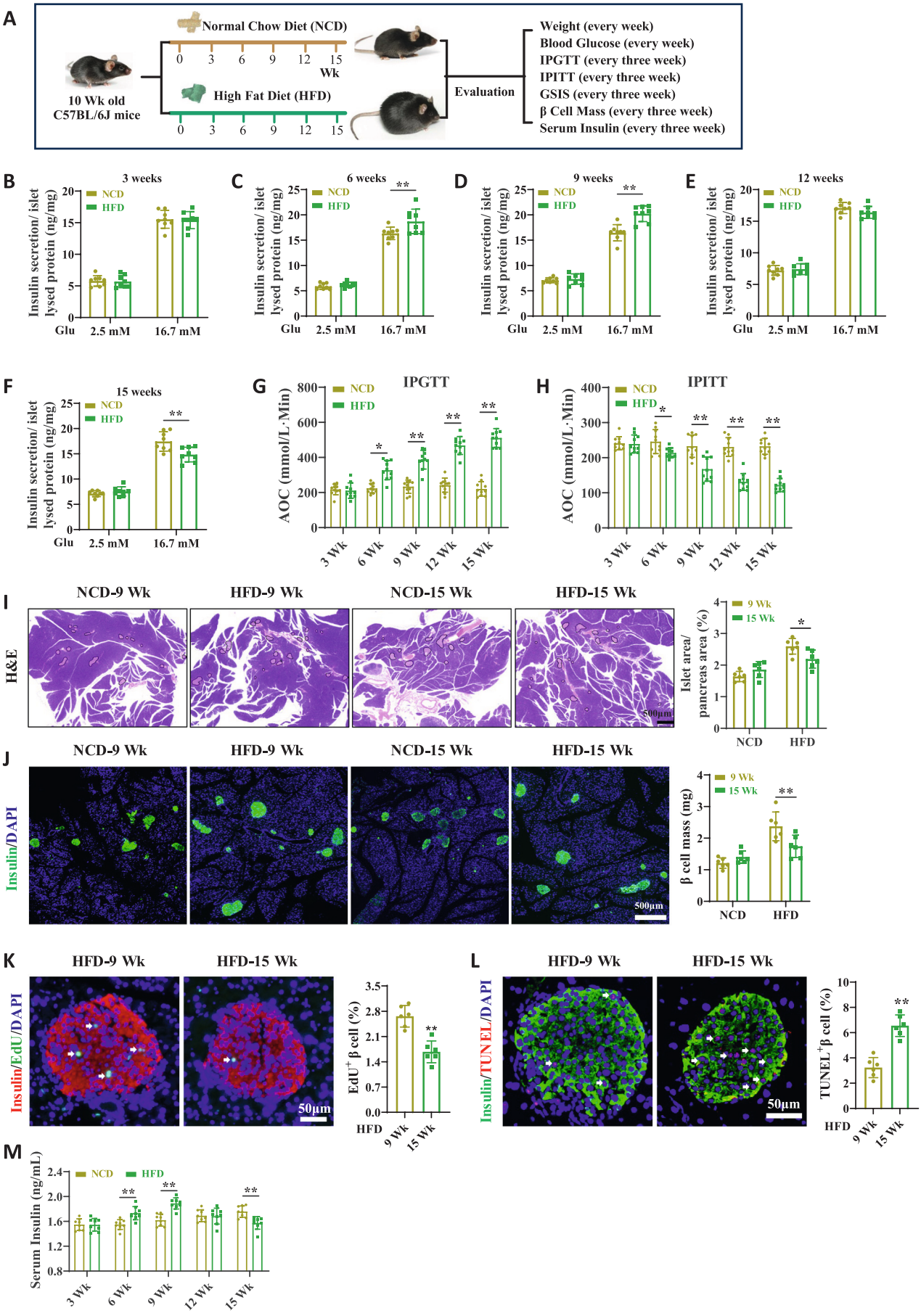

(caption on next page)

Fig. 1. Dynamic alterations of islet adaptation in response to continuous HFD feeding. (A) Schematic illustration of the experimental design. (B-F) Static insulin secretion of isolated islets under indicated glucose concentrations. Islets pooled from mice were aliquoted and stimulated with 2.5 mM or 16.7 mM glucose. Data were analyzed by independent-samples *t*-test ($n = 6$ mice per group); $^{*}p < 0.05$, $^{**}p < 0.01$; HFD vs. NCD. (G, H) Area of the curve (AOC) for IPGTT and IPITT. Data were analyzed by two-way ANOVA with multiple comparisons ($n = 10$ mice per group); $^{*}p < 0.05$, $^{**}p < 0.01$; HFD vs. NCD. (I) Representative H&E staining of pancreatic sections from mice fed an NCD or HFD for 9 or 15 weeks (left panel), and quantitative analysis of islet area percentage per pancreatic section (right panel; at least 6 sections per mouse, section interval: 100 μm). Scale bar = 500 μm. Data were analyzed by independent-samples *t*-test (n = 6 mice per group); $^{*}p < 0.05$; HFD-fed for 9 weeks vs. HFD-fed for 15 weeks. (J) Representative immunofluorescence staining of insulin (green) and DAPI (blue) in pancreatic sections from mice fed an NCD or HFD for 9 or 15 weeks (left panel), and quantification of β-cell mass (right panel; at least 6 sections per mouse, section interval: 100 μm). Scale bar = 500 μm. Data were analyzed by independent-samples *t*-test (n = 6 mice per group); $^{**}p < 0.01$; HFD-fed for 9 weeks vs. HFD-fed for 15 weeks. (*K*, *L*) Representative co-immunofluorescence staining of EdU (green, K) or TUNEL (red, L), together with insulin and DAPI, in pancreatic islets from HFD-fed mice at 9 and 15 weeks (left panel). White arrows indicate EdU^{+} or $TUNEL^{+}$ cells; Scale bar = 50 μm. Corresponding quantification of EdU^{+} $insulin^{+}$ cells and $TUNEL^{+}$ $insulin^{+}$ cells (right panel, no fewer than 8 islets per section were included for statistical analysis). Data were analyzed by independent-samples *t*-test (n = 6 mice per group); $^{**}p \leq 0.01$. (M) Serum insulin levels in mice fed an HFD for 3, 6, 9, 12 and 15 weeks, compared with age-matched NCD-fed control mice. Data were analyzed by two-way ANOVA with multiple comparisons ($n = 8$ mice per group); $^{**}p \leq 0.01$; HFD vs. NCD. (For interpretation of the references to colour in this figure legend, the reader is referred to the web version of this article.)

2.22. MSCs treatment in mice

HFD-induced obese mice with or without clodronate treatment were administered MSCs (2.5×10^{5} cells per mouse) via pancreatic capsule injection. Mice in the HFD control group and macrophage-depleted HFD group received vehicle treatment following the same schedule. IPGTT, IPITT, and serum insulin levels were assessed at 3-day intervals from 6 to 7 weeks after MSC administration.

2.23. Immunofluorescence

Paraffin-embedded pancreatic tissue sections and fixed cells were incubated with the following primary antibodies (Abcam) at a dilution of 1:400: Ki67 (ab15580), insulin (ab181547), TNFRI (ab223352), and β-catenin (ab305261). Samples were subsequently incubated with DyLight 594- or FITC-conjugated goat anti-rabbit IgG (ab96885 and ab6717, respectively). Fluorescence images were captured using a Zeiss LSM700 laser-scanning confocal microscope (Zeiss, Oberkochen, Germany) and quantified with ImagePro Plus 6.0 (Media Cybernetics, Silver Spring, MD, USA).

2.24. Cell transfection

MSCs were transfected with targeted lentivirus or control lentivirus (Suzhou Jima Biotechnology Co., Ltd., Suzhou, China) at the recommended concentration according to the manufacturer's instructions. Transfection efficiency was validated by RT-qPCR.

2.25. RT-qPCR

Total RNA was isolated using Trizol reagent (Takara, Cat# 9108). First-strand cDNA was synthesized with the 5 × All-In-One RT MasterMix (ABM, Cat# G490). Quantitative PCR was performed in a 10 μL reaction system using iTaq SYBR Green Supermix (Toyobo, Cat# QPK-201) on a Roche LightCycler 480 Real-Time PCR System (Roche, Basel, Switzerland). Relative gene expression was calculated using the $2^{-\Delta\Delta Ct}$ method, with values presented as the mean of at least three independent experiments and normalized to ACTB as the internal reference gene.

2.26. Western blot

Whole-cell lysates were prepared using RIPA buffer supplemented with 1% PMSF. Cytoplasmic and nuclear protein fractions were further isolated with a Nuclear and Cytoplasmic Protein Extraction Kit (Beyotime Institute of Biotechnology, Cat# P0027). Equal amounts of total protein, as well as cytoplasmic and nuclear protein fractions, were separated by 10% sodium dodecyl sulfate-polyacrylamide gel electrophoresis (SDS-PAGE) and transferred onto polyvinylidene fluoride (PVDF) membranes (Merck Millipore, Cat# ISEQ00010).

Membranes were blocked with 5% non-fat milk and incubated overnight with the indicated primary antibodies at a 1:2000 dilution: Wls (BioMérieux, orb417152), β-catenin (Abcam, ab305261), ACTB (Proteintech Group, 20536-1-AP), and Histone H3 (Proteintech, 17168-1-AP). Membranes were then probed with corresponding HRP-conjugated secondary antibodies. Protein blots were visualized using enhanced chemiluminescence (ECL) HRP substrate (Merck Millipore, Cat# WBULP-100ML) and imaged with a Tanon 5200 chemiluminescence imaging system (TANON Science & Technology Co., Ltd.).

2.27. Statistical analysis

For all in vivo and in vitro experiments, *n* indicates the number of biological replicates per group, as specified in the figure legends. No statistical method was used to predetermine the sample size. Statistical analyses were performed using SPSS 22.0. An independent Student's *t*-test was used for comparisons between two groups. One-way ANOVA followed by Tukey's HSD post hoc test was applied for multiple comparisons with equal variance, while Dunnett's post hoc test was used when equal variance was not assumed. Two-way ANOVA with Bonferroni's post hoc test was performed for bivariate comparisons. A value of $p < 0.05$ was considered statistically significant. Statistical graphs were generated using GraphPad Prism 8, and all results are presented as mean ± SD.

3. Results

3.1. Adaptation of β-cell from compensation to decompensation in obesity-induced diabetes

To characterize the dynamic changes in β-cell adaptation, C57BL/6J mice were subjected to a progressively HFD. This approach aimed to simulate the transition of β-cells from a state of compensation to one of decompensation (Fig. 1A). Consistent with our previous studies [27], prolonged HFD feeding led to continuous weight gain (Fig. S1A) and a steady rise in blood glucose (Fig. S1B). Glucose-stimulated insulin secretion (GSIS) from islets isolated from mice on an HFD or an NCD was evaluated every 3 weeks to assess the dynamic response of β-cells to glucose. We found a significant decrease in GSIS in islets from mice fed HFD for 15 weeks compared to those fed HFD for 9 weeks (Fig. 1B-F). This outcome was corroborated by continued changes in the area of the curve (AOC) [statistical method referred to [28]] from the IPGTT (Figs. 1G, S1C-1G) and IPITT (Figs. 1H, S1H-1L) assays, which are indicative of progressively worsening glucose tolerance and insulin sensitivity with HFD feeding. Compared to the NCD group, the relative area of the pancreatic islets was higher in HFD-fed mice but decreased after 15 weeks of HFD compared to 9 weeks of HFD (Fig. 1I). The β-cell mass exhibited a similar pattern (Fig. 1J). After 9 weeks of HFD feeding, the islets were relatively larger; however, their average size decreased

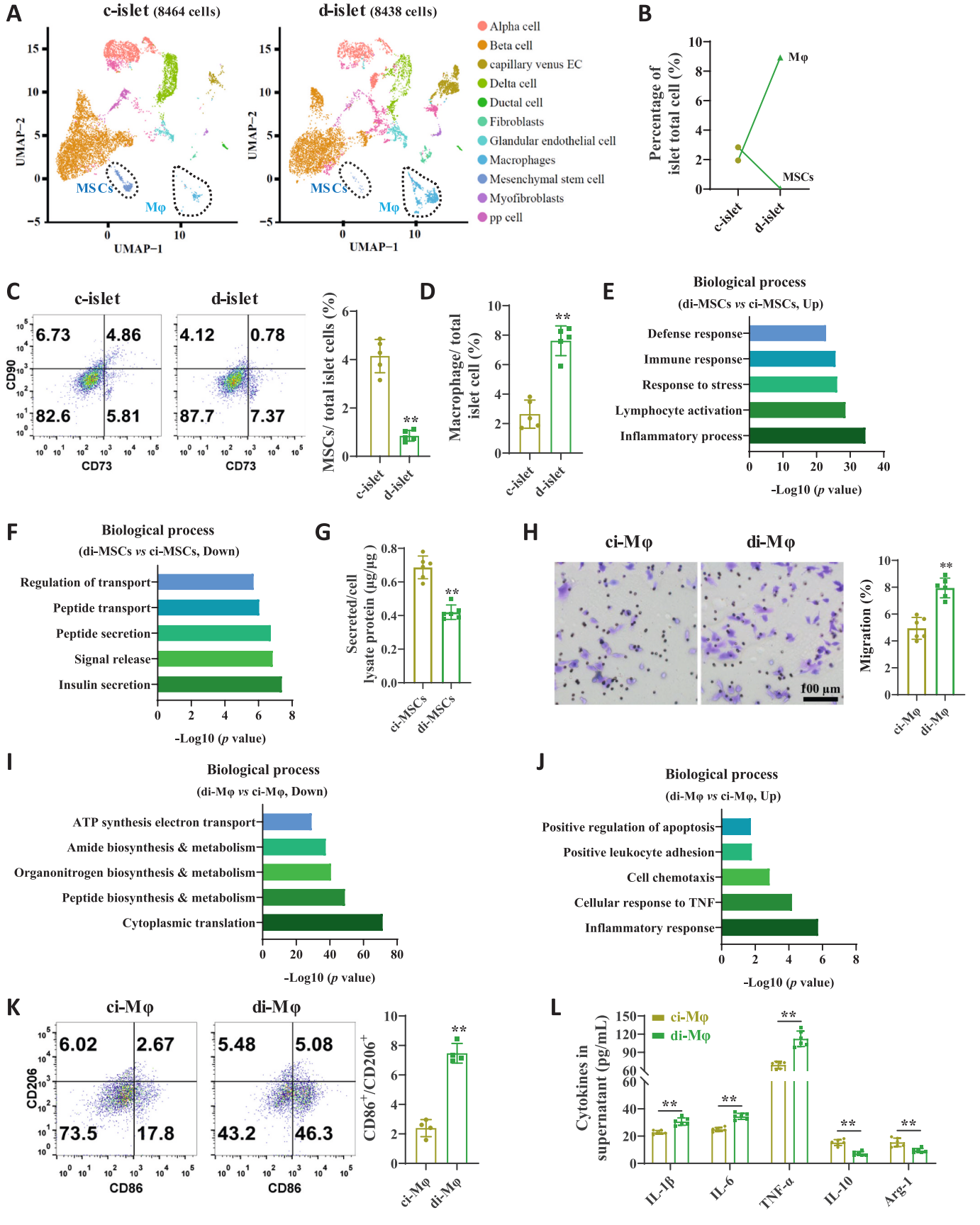

(caption on next page)

Fig. 2. Dynamic changes of MSCs and macrophages during islets adaptation. (A) UMAP plot of single-cell RNA-seq profiles from c-islet and d-islet cells, with each cell colored by cluster and annotated post hoc. Cells were pooled from islets of six individual mice. MSCs and macrophages are marked with dashed circles. c-islet: compensated islet; d-islet: decompensated islet; MSCs: mesenchymal stem cells; Mφ: macrophages. (B) Changes in the proportions of MSCs and Mφ in c-islets and d-islets based on UMAP cell cluster annotation. (C, D) Relative proportions of MSCs (C) and Mφ (D) in c-islets versus d-islets. At least 50 individual islets per mouse were analyzed by flow cytometry. Data were analyzed by independent-samples *t*-test ($n = 5$ mice per group); $^{**}p < 0.01$. (E, F) Top five enriched biological processes for upregulated (E) and downregulated (F) genes in di-MSCs compared with ci-MSCs. ci-MSCs: c-islet-derived MSCs; di-MSCs: d-islet-derived MSCs. Enrichment significance was determined by Fisher's exact test and presented as $-\log_{10}(p\text{-value})$. (G) Concentrations of secreted proteins in the supernatant of ci-MSCs and di-MSCs cultured under serum-free conditions. Data were analyzed by independent-samples *t*-test; MSCs were pooled from six individual mice per group; $^{**}p \leq 0.01$. (H) Representative Transwell migration images of ci-Mφ and di-Mφ (left), and quantification of migrated cells (right). Scale bar = 100 μm. Data were analyzed by independent-samples *t*-test; Mφ were pooled from six individual mice per group; $^{**}p \leq 0.01$. ci-Mφ: c-islet macrophages; di-Mφ: d-islet macrophages. (I, J) Top five enriched biological processes for downregulated (I) and upregulated (J) genes in di-Mφ versus ci-Mφ. Significance was calculated by Fisher's exact test and displayed as $-\log_{10}(p\text{-value})$. (K) Flow cytometric analysis of M1/M2 polarization (CD86/CD206) of ci-Mφ and di-Mφ (left), and quantification of the percentages of $CD86^+$ and $CD206^+$ cells (right). No fewer than 40 islets per mouse were used for flow cytometry. Data were analyzed by independent-samples *t*-test (n = 6 mice per group); $^{**}p \leq 0.01$. (L) Levels of representative cytokines in the culture supernatants of ci-Mφ and di-Mφ. Data were analyzed by independent-samples *t*-test; Mφ were pooled from six individual mice per group; $^{**}p \leq 0.01$.

after 15 weeks (Fig. S1M). Immunofluorescence staining revealed decreased β-cell proliferation (Fig. 1K) and increased β-cell apoptosis (Fig. 1L) after 15 weeks of HFD feeding. Islets from the 15-week HFD mice showed comparable reductions in proliferation and increases in apoptosis compared to age-matched NCD controls (Fig. S1N and S1O), suggesting that these pathological changes are primarily driven by metabolic stress rather than chronological aging. Fasting serum insulin levels reached the peak at 9 weeks of HFD feeding and then continuously decreased as obesity progressed (Fig. 1M). These temporal data indicate that islet adaptation collapses between 9 and 15 weeks of HFD feeding. Therefore, we selected these time points for the HFD-fed mice to represent the compensatory and decompensatory phases (referred to as c-mice and d-mice, respectively) in subsequent experiments.

3.2. Kinetics of islet MSC and macrophage from compensation to decompensation

To identify the cell types that contribute to β-cell adaptation, we applied single-cell RNA sequencing (scRNA-seq) on the islets. Single islet cells from c-mice (compensatory islet, hereafter referred to as c-islet) or d-mice (designated decompensatory islet, hereafter referred to as d-islet) underwent barcoding, library preparation, and sequencing using the 10 × Genomics pipeline (Fig. S2A). Employing a graph-based clustering approach, we profiled 8464 c-islet cells and 8638 d-islet cells, visualizing them in UMAP plots (Fig. 2A). Cell types were identified and assigned based on consensus hallmark genes, with each cluster corresponding to endocrine cells, macrophages, MSCs, or other recognized cell types (Figs. 2A, S2B). Notably, we observed a significant decrease in β-cell numbers in the d-islet (Figs. 2A, S2C), indicating a transition from compensated to decompensated phenotypes [29]. Compared to the c-islet, the d-islet showed a significant increase in macrophages (Mφ) (Figs. 2B, S2C), while the MSCs population declined (Figs. 2B, S2C). Flow cytometry was employed to further describe the dynamic changes of MSCs and Mφ in the islet from compensation to decompensation (Fig. S2D). Compared to the c-islet, there was a significant reduction in the proportion of MSCs within the d-islet (Fig. 2C). In contrast, age-matched NCD-fed mice displayed no significant differences in MSCs proportions (Fig. S2E). Unlike MSCs, the proportion of Mφ increased as the condition progressed from the compensatory to the decompensatory phase (Figs. 2D, S2F). Immunofluorescence staining further validated the elevated levels of pancreatic islet Mφ during the decompensated phase (Fig. S2G).

Next, we conducted an analysis of the phenotypes and biological functions of MSCs and Mφ within the islets during the transition from compensation to decompensation. Compensatory islet MSCs will be designated as ci-MSCs, while compensatory islet macrophages will be referred to as ci-Mφ. Conversely, decompensatory islet MSCs and macrophages will be denoted as di-MSCs and di-Mφ, respectively. We found that di-MSCs are more likely to differentiate into adipocytes, but their osteogenic and chondrogenic abilities were reduced (Fig. S2H). Nevertheless, their surface markers still comply with the criteria for MSCs (Fig. S2I). Furthermore, the proliferation and migratory ability of di-MSCs decreased (Fig. S2J and S2K), while the senescence phenotype increased compared with ci-MSCs (Fig. S2L). Gene ontology analysis revealed that, compared to ci-MSCs, the upregulated genes in di-MSCs were predominantly associated with immune system processes (Fig. 2E). In contrast, the downregulated genes were mainly linked to peptide and protein transport processes (Fig. 2F). Consistent, the protein concentration in the di-MSCs supernatant decreased compared with the ci-MSCs supernatant (Fig. 2G), indicating a reduction in paracrine ability during the decompensated phase. Unlike MSCs, there was no significant change in the proliferation of Mφ during the decompensated phase (Fig. S2M), but their migration was enhanced (Fig. 2H). Compared with ci-Mφ, the downregulated genes in di-Mφ were enriched in organonitrogen and amide metabolism (Fig. 2I), while the upregulated genes were associated with the inflammatory response biological process (Fig. 2J). This indicates that Mφ in the decompensated phase exhibit more intense inflammation than those in the compensated phase. Consistent with this, the di-Mφ exhibited an M1-like phenotype (Fig. 2K). Changes in cytokine levels in the culture supernatant reinforce the phenotypic conversion of Mφ during the transition from compensatory to decompensated stages (Fig. 2L).

3.3. Infiltrated macrophage governs islet MSC during decompensation

Given that di-Mφ demonstrate an increased migratory capacity rather than a proliferation capability, we propose that the rise in d-islet macrophages is primarily due to the recruitment of peripheral cells. Macrophages from EGFP driven by the actin promoter were injected into 9- and 15-week-old mice fed a HFD via the tail vein. A higher proportion of EGFP-positive macrophages was detected in the islets of 15-week-old mice compared to those fed an HFD for 9 weeks, as determined by immunofluorescence and flow cytometry (Fig. 3A and B). Conversely, age-matched mice fed a NCD exhibited substantially fewer EGFP-positive macrophages in their pancreatic islets than their HFD counterparts, and this low level of infiltration remained consistent across ages (Fig. S3A and S3B). Immunofluorescence and ELISA analyses revealed that d-islets show higher CCL2 expression and multiple chemokine levels compared to age-matched NCD-fed mice (Figs. 3C and D, S3C and S3D). To reveal the cell type responsible for the dynamic shifts in adaptive islet macrophages, co-culture assays were conducted to quantify macrophage recruitment. As previously reported, di-β-cells possess a greater capacity for macrophage migration compared to ci-β-cells (Fig. 3E). Notably, di-MSCs also exhibited enhanced macrophage chemotaxis (Fig. 3F), which can be attributed to increased chemokine levels (Fig. 3G). In contrast, chemokine levels in MSCs derived from NCD-fed mice were lower and remained stable over time (Fig. S3E). Therefore, we further assessed the impact of these cells on the transition of macrophage phenotype. The results showed that di-β-cells had no significant effect on the inflammatory phenotype transition of Mφ

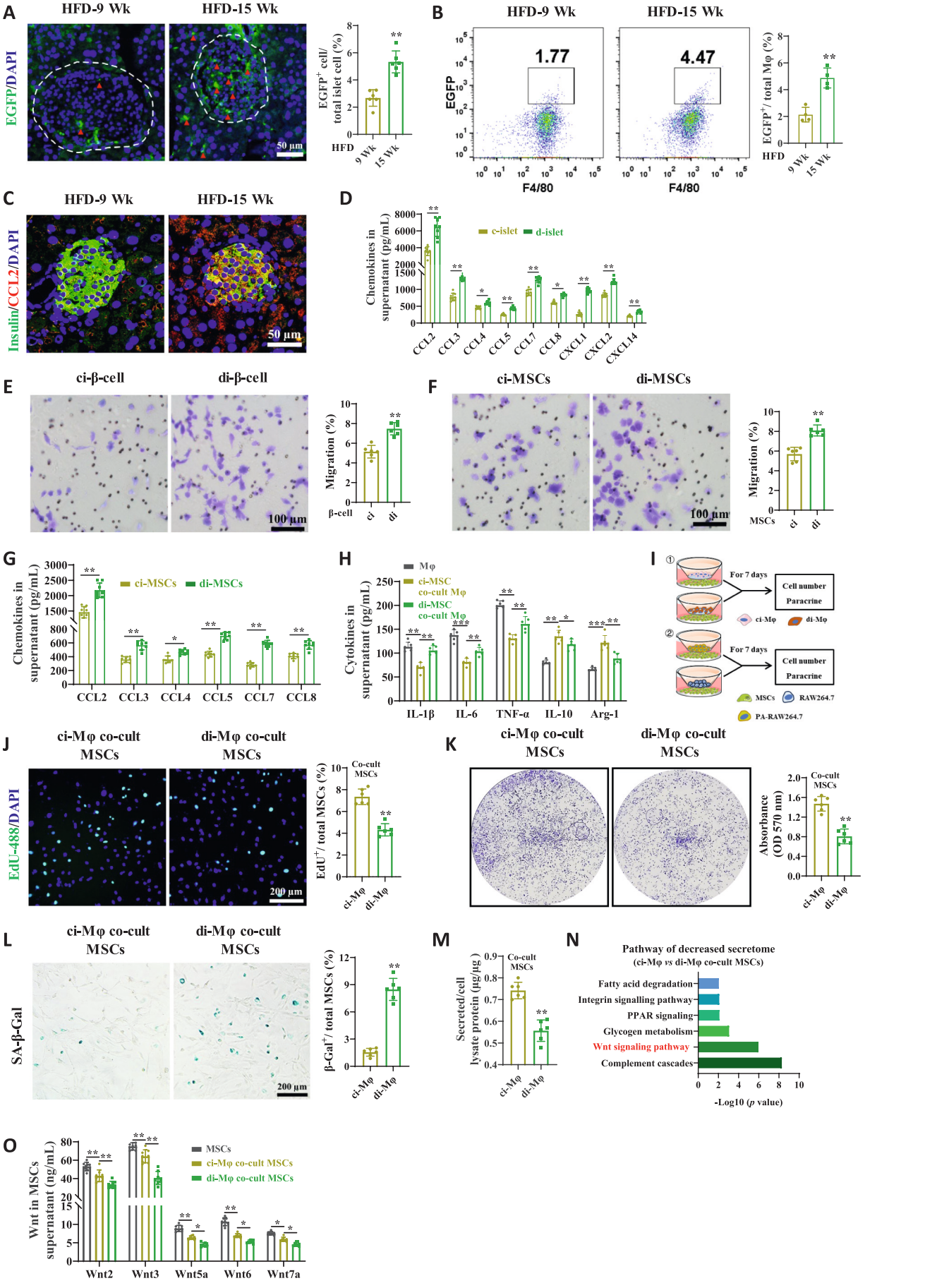

(caption on next page)

Fig. 3. Infiltrated macrophage governs MSC conversion during islet adaptation. (A) Representative immunofluorescent images showing the accumulation of transferred EGFP$^+$ macrophages in pancreatic islets from mice fed a HFD for 9 and 15 weeks (left), and quantification of EGFP$^+$ cells within the islets (right; at least 8 islets were counted per section). Scale bar = 50 μm. Data were analyzed using an independent-samples *t*-test ($n = 4$ mice per group); $^{**}p < 0.01$. (B) Flow cytometric analysis of transferred EGFP$^+$ macrophages in islets from HFD-fed mice at 9 and 15 weeks of age (left), and the corresponding quantification of EGFP$^+$ macrophages (right; no fewer than 40 islets per mouse were collected for flow cytometry). Data were analyzed using an independent-samples *t*-test (n = 4 mice per group). $^{**}p \leq 0.01$. (C) Representative immunofluorescent images of CCL2 expression in pancreatic islets from compensated and decompensated mice. Scale bar = 50 μm; n = 4 individual mice per group. (D) Levels of chemokines in the culture supernatant of c-islets and d-islets. Data were analyzed using an independent-samples *t*-test ($n = 8$ mice per group). $^{*}p \leq 0.05$, $^{**}p \leq 0.01$. (E) Representative images of Transwell migration assays for macrophages co-cultured with ci-β-cells or di-β-cells (left), and corresponding quantitative analysis of migrated cells (right). Scale bar = 100 μm. Data were analyzed using an independent-samples *t*-test; macrophages and β-cells were each isolated from 6 individual mice. $^{**}p \leq 0.01$. ci-β-cell: compensated islet β-cell; di-β-cell: decompensated islet β-cell. (F) Representative images of Transwell migration assays for macrophages co-cultured with ci-MSCs or di-MSCs (left), and corresponding quantification of migrated cells (right). Scale bar = 100 μm. Data were analyzed using an independent-samples *t*-test; MSCs were isolated from 6 individual mice. $^{**}p \leq 0.01$. (G) Chemokine levels in the culture supernatant of ci-MSCs and di-MSCs. Data were analyzed using an independent-samples *t*-test; MSCs were pooled from 6 individual mice. $^{**}p \leq 0.01$. (H) Cytokine levels in the culture supernatant of Mφ co-cultured with ci-MSCs or di-MSCs. Data were analyzed using one-way ANOVA with Tukey's HSD post hoc test; MSCs were each isolated from 6 individual mice. $^{*}p \leq 0.05$, $^{**}p \leq 0.01$, $^{***}p \leq 0.001$. (I) Schematic diagram of the co-culture system. MSCs (seeded in the lower chamber) were co-cultured with Mφ or RAW264.7 cells at a 1:2 ratio (MSCs: macrophages) and incubated for 7 days. Subsequently, the proliferation and secretory function of MSCs were assessed. PA-RAW264.7: palmitic acid-pretreated RAW264.7 cells. (J-L) Representative images of MSCs proliferation (J), colony formation (K), and senescence (L) after co-culture with ci-Mφ or di-Mφ (left), and corresponding quantitative results (right). Scale bar = 200 μm. Data were analyzed using an independent-samples *t*-test; MSCs and Mφ were each isolated from 6 individual mice. $^{**}p \leq 0.01$. (M) Total protein concentration in FBS-free culture supernatant of MSCs co-cultured with ci-Mφ or di-Mφ. Data were analyzed using an independent-samples *t*-test; MSCs and macrophages were each isolated from 6 individual mice. $^{**}p \leq 0.01$. (N) Top 6 significantly downregulated signaling pathways enriched by proteomic sequencing of the supernatant from MSCs co-cultured with ci-Mφ versus di-Mφ. (O) Wnt levels in the culture supernatant of MSCs co-cultured with ci-Mφ or di-Mφ. Data were analyzed using one-way ANOVA with Tukey's HSD post hoc test; MSCs and Mφ were each isolated from 6 individual mice. $^{**}p \leq 0.01$.

(Fig. S3F), similar to the effect observed with β-cells from NCD-fed mice (Fig. S3G). However, Mφ co-cultured with di-MSCs exhibited higher levels of pro-inflammatory cytokines than ci-MSCs (Fig. 3H), a pattern not observed in MSCs from NCD mice (Fig. S3H). Both PA-pretreated MIN6 cells and MSCs showed similar regulatory patterns concerning Mφ migration and inflammation (Fig. S3I-S3L). These results suggest that β-cells and MSCs collaborate to recruit macrophages, which are responsible for the phenotypic transformation of di-Mφ in the islet during the decompensatory phase.

Next, we will employ a co-cultivation system to investigate which cell type induces dynamic changes in adaptive islet MSCs. Given the predominance of β-cells in pancreatic islets, we first assessed their influence on MSCs function using a Transwell co-culture system (Fig. S3M). Considering the substantial presence of macrophages, we also evaluated their effect on MSCs using the same method (Fig. 3I). The co-culture results showed that di-Mφ significantly inhibited MSCs proliferation and clone formation, inducing senescence (Fig. 3J-L), while simultaneously reducing their paracrine capacity (Fig. 3M). However, co-culturing with β-cells or PA-pretreated MIN6 cells did not alter the aforementioned phenotypes in MSCs (Fig. S3N-S3U). A similar pattern was observed in PA-pretreated RAW 264.7 macrophages (Fig. S3V-S3Y). Due to the decreased paracrine secretion from MSCs co-cultured with di-Mφ, we explored the species attribution of these proteins through proteomic sequencing of the supernatants from di-Mφ co-cultured MSCs. The GO enrichment analysis indicated that the reduced secreted proteins were primarily enriched in the Wnt signaling pathway (Fig. 3N). An ELISA assay further validated that Wnt levels were significantly decreased in the MSCs supernatant when co-cultured with di-Mφ (Fig. 3O). Nonetheless, di-Mφ exhibited only a minimal impact on Wnt transcription (Fig. S3Z). Similarly, reduced extracellular transport of Wnt, but not transcription, was observed in PA-pretreated RAW264.7 co-cultured MSCs (Fig. S3AA and S3AB). These results indicate that the transition of MSCs from a compensatory state to decompensation was predominantly influenced by macrophage infiltration and a change in metabolic profile during the decompensation phase.

3.4. Macrophage-derived TNF-α regulates MSC Wnt secretion by inhibiting Wls

To investigate the macrophage-derived factors responsible for the phenotypic transition of MSCs, we compared the secretory profiles of macrophages from c-islets and d-islets. According to scRNA-seq, we observed that TNF-α, a key marker of pro-inflammatory macrophages known to impair β-cell function, was significantly elevated in di-Mφ (Fig. 4A). ELISA results further showed that di-Mφ exhibited higher levels of inflammatory cytokines, with TNF-α demonstrating the greatest increase and highest concentration in the culture supernatant (Fig. 4B). A similar pattern of elevated cytokines was noted in d-islets (Fig. 4C). Depleting macrophages with clodronate liposomes significantly reduced inflammatory cytokine levels in d-islets, with TNF-α showing the most substantial decrease (Fig. 4D). These findings suggest that macrophages are the primary source of inflammatory mediators in the islet, with TNF-α being the predominant secreted cytokine.

Next, we sought to determine whether macrophage-derived TNF-α is the key factor altering MSCs function. As expected, 50 ng/mL of TNF-α inhibited MSCs proliferation, clone formation, and Wnt secretion while inducing senescence (Fig. 4E-H). Notably, di-MSCs expressed elevated levels of TNF-α receptor 1 (TNFR1) (Fig. 4I), although the underlying mechanism remains unclear. Given that TNF-α does not inhibit Wnt transcription (Fig. S4A), we then investigated how macrophage-derived TNF-α inhibits Wnt secretion in MSCs. Considering the downregulation of di-MSCs genes enriched in protein transport (Fig. 2F) and the known Wnt secretion mechanism, we speculated that TNF-α's reduction in Wnt secretion might be related to decreased extracellular transport. Reanalyzing the scRNA-seq results revealed that Wls, the key protein mediating Wnt's extracellular transport [30], was decreased in di-MSCs (Fig. S4B). Protein and mRNA analyses confirmed a reduction in Wls levels in di-MSCs (Fig. 4J and K).

These findings prompted us to investigate whether TNF-α can regulate Wls. As expected, treatment with 50 ng/mL of TNF-α inhibited the transcription and expression of Wls in MSCs (Fig. 4L and M). Consistent with previous reports, knocking down *Wls* reduced the secretion of certain Wnts in MSCs (Fig. S4C). Furthermore, a functional rescue experiment demonstrated that TNF-α inhibits Wnt secretion in a Wls-dependent manner (Fig. S4D and S4E). Since *Wls* is not a direct downstream target gene of TNF-α, we explored the regulatory factors mediating the interaction between TNF-α and Wls. Using prediction tools for *Wls* transcription factors and TNF-α downstream genes, we identified seven potential candidates: IRF1, IRF3, STAT5A, JUN, FOS, CEBP, and USF2 (Fig. 4N). RT-qPCR revealed that four of these candidates were regulated by TNF-α in MSCs (Fig. S4F). In forced expression experiments, we found that only IRF3 overexpression inhibited Wls expression, while IRF1, STAT5A, and JUN did not have this effect in MSCs (Fig. 4O). A dual luciferase reporter assay further confirmed that IRF3 could bind to the *Wls* promoter, exerting a negative regulatory effect (Fig. 4P). Consistently, following *IRF3* overexpression, Wnt secretion

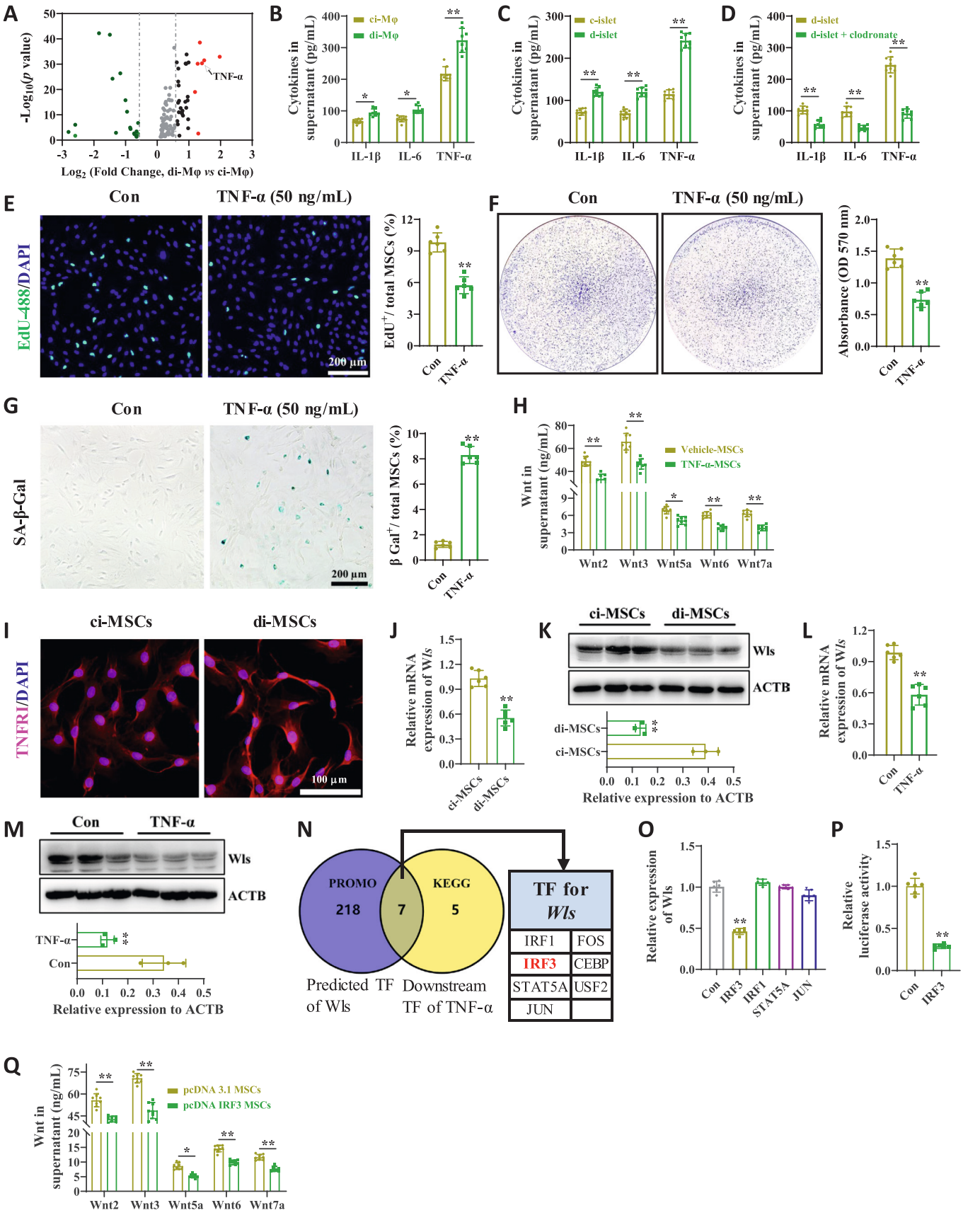

(caption on next page)

Fig. 4. Macrophage-derived TNF-α regulates MSC Wnt secretion by inhibiting Wls. (A) Volcano plots derived from single-cell RNA-seq comparing di-Mφ with ci-Mφ based on Hallmark gene sets. Top upregulated and downregulated genes encoding secretory proteins with $p < 0.05$ are labeled; *Tnf-α* is highlighted. (B) Cytokine levels in the culture supernatant of ci-Mφ and di-Mφ. Data were analyzed by independent-samples *t*-test (Mφ isolated from 8 individual mice per group); $^{*}p \leq 0.05$, $^{**}p \leq 0.01$. (C) Cytokine levels in the culture supernatant of c-islets and d-islets. Data were analyzed by independent-samples *t*-test (n = 8 mice per group); $^{**}p \leq 0.01$. (D) Cytokine levels in the supernatant of d-islets following clodronate treatment. At least 40 islets per mouse were aliquoted and treated with vehicle or clodronate for 48 h. Data were analyzed by independent-samples *t*-test (n = 8 mice per group); $^{**}p \leq 0.01$. (*E*-G) Representative images of MSCs proliferation (E), colony formation (F), and senescence (G) after TNF-α treatment (left), with corresponding quantitative analyses (right). Scale bar = 200 μm. Data were analyzed by independent-samples *t*-test (MSCs isolated from 6 individual mice per group); $^{**}p \leq 0.01$. (H) Wnt levels in the culture supernatant of TNF-α-treated MSCs. Data were analyzed by independent-samples *t*-test (MSCs isolated from 8 individual mice per group); $^{*}p \leq 0.05$, $^{**}p \leq 0.01$. (I) Representative immunofluorescence staining of TNFR1 in MSCs. TNFR1 (red), DAPI (blue). Scale bar = 100 μm. MSCs were isolated from 4 individual mice. (J) *Wls* transcript levels in ci-MSCs and di-MSCs. Data were analyzed by independent-samples *t*-test (MSCs isolated from 6 individual mice per group); $^{**}p < 0.01$. (K) Wls protein levels in ci-MSCs and di-MSCs. Data were analyzed by independent-samples *t*-test (MSCs isolated from 3 individual mice per group); $^{**}p < 0.01$. (L) *Wls* mRNA expression in TNF-α-treated MSCs. Data were analyzed by independent-samples *t*-test (MSCs isolated from 6 individual mice); $^{**}p < 0.01$. (M) Wls protein levels in TNF-α-treated MSCs. Data were analyzed by independent-samples *t*-test (MSCs isolated from 6 individual mice); $^{**}p < 0.01$. (N) Venn diagram showing the overlap between Wls-related transcription factors and TNF-α downstream genes predicted using PROMO and KEGG databases, respectively. (O) Relative expression of candidate transcription factors regulating *Wls*. Data were analyzed by one-way ANOVA ($n = 6$); $^{**}p \leq 0.01$. (P) Relative luciferase activity in 293 T cells co-transfected with pGL3-Luc::*Wls* and pcDNA3.1-IRF3 or empty pcDNA3.1 vector. Data were analyzed by independent-samples *t*-test (n = 6); $^{**}p < 0.01$. (Q) Wnt levels in the supernatant of MSCs transfected with pcDNA3.1-IRF3. Data were analyzed by independent-samples *t*-test (MSCs isolated from 8 individual mice per group); $^{*}p \leq 0.05$, $^{**}p \leq 0.01$. (For interpretation of the references to colour in this figure legend, the reader is referred to the web version of this article.)

decreased in MSCs (Fig. 4Q), mirroring the results of TNF-α treatment. TNF-α stimulation, combined with *IRF3* knockdown, neutralized the decline in Wls expression and Wnt secretion in MSCs (Fig. S4G-S4I). These data demonstrate that macrophage-derived TNF-α modulates Wnt secretion in MSCs via the IRF3/Wls axis, ultimately driving the transition of MSCs function from compensation to decompensation.

3.5. Impaired Wnt secretion weakens the regulatory capacity of MSCs on macrophages and β cells

Given the trophic support MSCs provide to β-cells and their immunosuppressive role in maintaining tissue homeostasis, we next explored whether and how MSCs impairment contributes to the conversion of islet function from compensation to decompensation. To address the limited quantity of di-MSCs and their reduced Wnt secretion, we developed Wls knockdown MSCs (*shWls*-MSCs) to replicate the di-MSCs phenotype. In a co-culture system, our findings revealed that *shWls*-MSCs, when co-cultured with primary macrophages and RAW264.7 cells, produced significantly higher levels of inflammatory cytokines compared to the empty vector control (*shCon*-MSCs) (Figs. 5A, S5A). Additionally, the results of the Seahorse XF96 Cell Mito Stress Test showed that *shWls*-MSCs co-cultured with primary macrophages had a lower oxygen consumption rate (Fig. 5B), basal respiration (Fig. 5C), maximal respiration (Fig. 5D), proton leak (Fig. 5E), and ATP biosynthesis (Fig. 5F). Similar trends were observed in *shWls*-MSCs and *shCon*-MSCs co-cultured with RAW264.7 cells (Fig. S5B-S5F). Furthermore, *shWls*-MSCs co-cultured with primary macrophages and RAW264.7 cells showed increased ROS levels compared to those co-cultured with *shCon*-MSCs (Figs. 5G, S5G). These findings suggest that during the decompensated period, converted MSCs had a reduced capacity to regulate macrophage inflammatory responses compared to compensatory MSCs. We will next attempt to elucidate the molecular mechanism by which MSCs induce conversion of the macrophage phenotype. Given the observed downregulation of Wnt secretion in di-MSCs, we hypothesize that MSCs may influence macrophage activity via the Wnt signaling pathway. Our co-culture experiments indicate that *shCon*-MSCs significantly enhance the nuclear translocation of β-catenin in both primary macrophages and RAW264.7 cells. In contrast, this effect is markedly diminished in the presence of *shWls*-MSCs (Figs. 5H, S5H). Co-cultivation with *shWls*-MSCs decreased the expression of Wnt pathway genes, including *Pparδ*, *Pparγ*, *c-Myc,* and *Tgf-β*, in both primary macrophages and RAW264.7 cells (Figs. 5I, S5I). Furthermore, the oxidative phosphorylation phenotype was decreased in *Pparδ*-deficient primary macrophages and RAW264.7 cells co-cultured with MSCs (Figs. 5J, S5J), and the inflammatory cytokines in a similar pattern (Figs. 5K, S5K). These results indicate that during the compensated stage of diabetes, MSCs regulate the metabolic phenotype of macrophages via the β-catenin/PPARδ pathway. In contrast, during the decompensated stage, reduced Wnt secretion by MSCs diminishes this regulatory capacity, thus impairing tissue homeostasis.

We next analyzed the role of impaired MSCs in the transition from β-cell adaptation to T2DM decompensation. Using a co-culture strategy, we discovered that *shWls*-MSCs reduce β-catenin nuclear translocation in primary islet β-cells and MIN6 cells (Figs. 5L, S5L). Results from nuclear-cytoplasmic separation further confirm that *shCon*-MSCs preferentially promote β-catenin nuclear translocation in islet β-cells and MIN6 cells (Figs. 5M, S5M). Transcription of several β-catenin downstream genes was decreased in islet β-cells and MIN6 cells co-cultured with *shWls*-MSCs compared to cells co-cultured with *shCon*-MSCs (Figs. 5N, S5N). Consistent with Wnt pathway activation, proliferation of pancreatic islet β-cells and MIN6 cells was reduced (Figs. 5O, S5O), while apoptosis concurrently increased (Figs. 5P, S5P). Additionally, di-MSCs inhibited Ca^{2+} influx and insulin secretion in primary β-cells (Fig. 5Q and R), a pattern similar to that observed in MIN6 cell lines co-cultured with *shWls*-MSCs (Fig. S5Q and S5R). These results suggest that altered MSCs numbers, functions, and properties, particularly the decreased secretion of Wnt, contribute to the functional shift of β-cells from a compensatory state to decompensation.

3.6. MSC administration combined with macrophage deletion reversing β-cell decompensation

Based on these findings, we explored whether the concurrent administration of MSCs and macrophage deletion could reverse β-cell decompensation in diabetic mice. Following 15 weeks on an HFD, the mice were categorized into four groups: negative control (NC), macrophage clearance (cl-Mφ), MSCs alone (MSCs), and macrophage clearance with MSC injection (cl-Mφ + MSCs). The experimental process is shown in Fig. 6A. There were no significant differences in weight or food intake among the groups during the study period (Fig. S6A and S6B). As expected, clodronate successfully depleted macrophages in the islets (Fig. 6B) and other organs (Fig. S6C-S6G). Pancreatic capsule-injected MSCs quickly homed to the islets and persisted within the pancreatic parenchyma for extended periods (Fig. 6C and D). The cl-Mφ + MSCs group showed a decrease in serum blood glucose and an increase in insulin content, demonstrating greater efficacy than the MSCs-alone group (Fig. 6E and F). Meanwhile, depletion of macrophages or administration of MSCs alone suppressed serum TNF-α, IL-1β, and IL-6; these cytokines were further reduced in the cl-Mφ + MSCs group (Fig. 6G). An ELISA assay showed that certain Wnts increased in the serum of the MSCs alone and cl-Mφ + MSCs groups, but this was not observed in the cl-Mφ group (Fig. 6H). Compared to the cl-Mφ and MSCs alone groups, cl-Mφ + MSCs promoted β-cell proliferation and inhibited their apoptosis (Fig. 6I and J). Additionally, the cl-Mφ + MSCs group

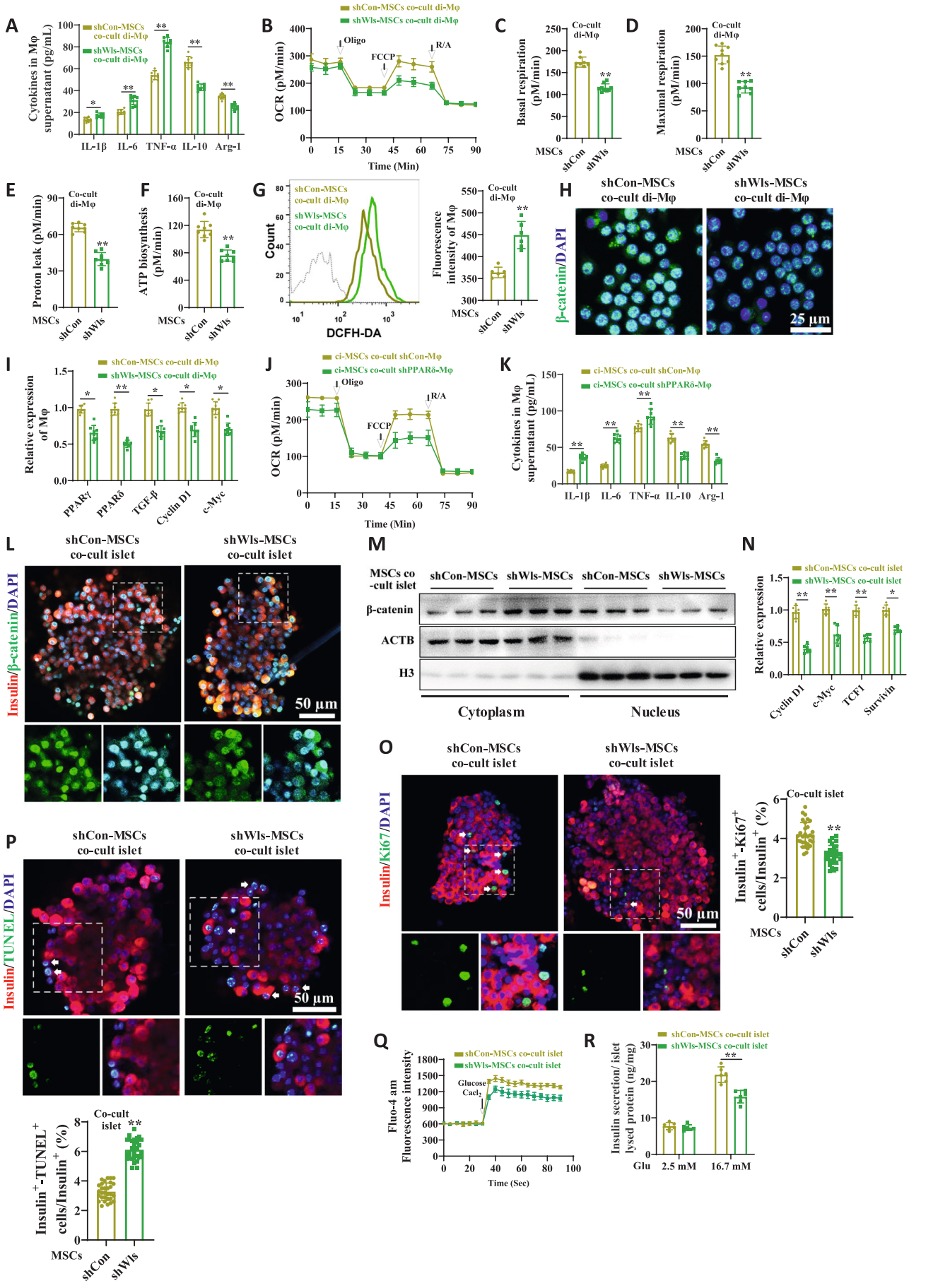

(caption on next page)

Fig. 5. Wnt secretion impairment weakens the regulatory capacity of MSC in macrophage and β-cell adaptation. (A) Cytokine levels in the culture supernatant of Mφ co-cultured with sh*Con*-MSCs or sh*Wls*-MSCs. Data were analyzed by independent-samples *t*-test (di-Mφ isolated from 8 individual mice per group); $*p \leq 0.05$, $**p \leq 0.01$. (B—F) Oxygen consumption rate (OCR) reflecting cellular energy metabolism in Mφ co-cultured with sh*Con*-MSCs (yellow) or sh*Wls*-MSCs (green). OCR was measured under basal conditions and after sequential treatment with oligomycin, FCCP, and rotenone plus antimycin A (RA). Basal respiration (C), maximal respiration (D), proton leak (E), and ATP production (F) were calculated accordingly. Data were analyzed by independent-samples *t*-test (Mφ isolated from 8 individual mice per group); $**p \leq 0.01$. (G) Intracellular ROS levels in Mφ co-cultured with sh*Con*-MSCs (yellow) or sh*Wls*-MSCs (green). Data were analyzed by independent-samples *t*-test (Mφ isolated from 6 individual mice per group); $**p \leq 0.01$. (H) Representative immunofluorescence images of β-catenin nuclear translocation in Mφ co-cultured with sh*Con*-MSCs or sh*Wls*-MSCs. Scale bar = 25 μm. Mφ were isolated from 4 individual mice. (I) Expression of downstream genes in the Wnt/β-catenin signaling pathway in Mφ co-cultured with sh*Con*-MSCs or sh*Wls*-MSCs. Data were analyzed by independent-samples *t*-test (Mφ isolated from 6 individual mice per group); $*p \leq 0.05$, $**p \leq 0.01$. (J) OCR profiles of sh*Pparδ*-Mφ (green) and sh*Con*-Mφ (yellow) co-cultured with MSCs. Mφ were isolated from 8 individual mice. (K) Cytokine levels in sh*Pparδ*-Mφ (green) and sh*Con*-Mφ (yellow) co-cultured with MSCs. Data were analyzed by independent-samples *t*-test (Mφ isolated from 8 individual mice per group); $**p \leq 0.01$. (L) Representative images of β-catenin nuclear translocation in isolated islets co-cultured with sh*Con*-MSCs or sh*Wls*-MSCs. Scale bar = 50 μm. Islets were isolated from 3 individual mice. (M) Cytosolic and nuclear protein levels of β-catenin in islets co-cultured with sh*Con*-MSCs or sh*Wls*-MSCs. Islets were isolated from 3 individual mice. (N) Expression of downstream genes in the Wnt/β-catenin signaling pathway in isolated islets co-cultured with sh*Con*-MSCs or sh*Wls*-MSCs. Data were analyzed by independent-samples *t*-test (islets isolated from 6 individual mice per group); $**p \leq 0.01$. (O, P) Proliferation and apoptosis of β-cells assessed by Ki67 staining (O) and TUNEL assay (P) in isolated islets co-cultured with sh*Con*-MSCs or sh*Wls*-MSCs (left), with corresponding quantitative analysis (right; no fewer than 30 islets per group were included for statistical analysis). Scale bar = 50 μm. Data were analyzed by independent-samples *t*-test (islets isolated from 6 individual mice per group); $**p \leq 0.01$. (Q) Ca^{2+} influx in isolated islets co-cultured with sh*Con*-MSCs or sh*Wls*-MSCs. Islets were isolated from 6 individual mice. (R) Insulin secretion from isolated islets co-cultured with sh*Con*-MSCs or sh*Wls*-MSCs at the indicated glucose concentrations. Data were analyzed by independent-samples *t*-test (islets isolated from 6 individual mice per group); $**p \leq 0.01$. (For interpretation of the references to colour in this figure legend, the reader is referred to the web version of this article.)

reduced the homeostatic model assessment of insulin resistance (HOMA-IR) values (Fig. 6K). Consistent with this, glucose tolerance and insulin sensitivity improved in the cl-Mφ + MSCs group (Fig. S6H-S6K). Finally, we isolated islets from all treatment groups. GSIS results showed improved insulin release across all groups, with the greatest improvement in the cl-Mφ + MSCs group (Fig. 6L). Building on the characterized interaction between MSCs and macrophages, we examined its impact on the functional transition of β-cells in vitro. Consistent with the report by Dr. Fu et al. [31], the proliferation and insulin secretion of β-cells were diminished in the presence of di-Mφ compared to ci-Mφ (Fig. 6M). Furthermore, di-Mφ were observed to induce apoptosis in β-cells (Fig. 6N). Consistently, the supplementation of ci-MSCs has been shown to mitigate the damage inflicted on islet β-cells by di-Mφ (Fig. 6M and N), as well as to enhance insulin secretion (Fig. 6P). These results indicate that the interaction between MSCs and macrophages plays a synergistic role in the transformation of β-cell function from a compensated to a decompensated state due to obesity.

4. Discussion

β-cell plasticity is a critical determinant of type 2 diabetes progression [32,33]. However, the dynamic natural adaptation of β-cells remains largely unexplored. Here, we examine how communication between MSCs and macrophages influences β-cell function and the shift from compensation to decompensation in T2DM. The intricate relationship between macrophages and MSCs is a crucial factor influencing β-cell fate and the progression of diabetes. Unfortunately, this delicate equilibrium is disrupted when islet macrophage infiltration increases and their inflammatory phenotype shifts (Graphical abstract). Our findings reveal a molecular and cellular mechanism that underlies the transformation of β-cell function and the transition from compensation to decompensation in diabetes. This mechanism involves interactions among β-cells, islet-resident MSCs, and macrophages, highlighting the central role of macrophage-MSC interactions in β-cell adaptation during diabetes.

In diabetes, macrophages negatively affect β-cells. Depleting macrophages reduces systemic inflammation and insulin resistance in HFD mice [11,34], despite several studies reporting that macrophages signal β-cell adaptive expansion [31,35]. Contradictory effects may arise from the varying phenotypes of macrophages at different stages of the disease [36]. This study shows that decompensated-islet macrophages produce increased pro-inflammatory cytokines, which negatively affect β-cell insulin secretion and insulin sensitivity, particularly through IL-6 and TNF-α [37,38]. Meanwhile, this unfavorable effect may be generalizable to a wide range of neighboring cells [39]. Previous studies have shown that the number of MSCs is diminished and their clonogenic capacity is compromised in ex vivo bone marrow aspirates obtained from individuals with diabetes [40,41]. This study demonstrates, for the first time, that local endogenous MSCs populations within the islets are diminished during decompensation relative to compensation, thereby impairing β-cell adaptive processes. Pro-inflammatory macrophages infiltrate the islet microenvironment, significantly contributing to the depletion of the MSC pool. This occurs through the promotion of MSC apoptosis and senescence via TNF-α signaling, ultimately diminishing β-cell secretory capacity.

The roles of MSCs in regulating tissue restoration and regeneration include differentiation and providing trophic support to neighboring cells through multidirectional interactions [14,20]. In pancreatic islets, endogenous MSCs provide direct trophic support to islet cells. Co-transplantation of MSCs with pancreatic islets significantly increases the survival of transplanted islets and attenuates their apoptosis [17,42]. In our experiments, the protective effect of MSCs on islets and β-cells was also observed, as reported [39]. Co-culturing MSCs significantly enhances islet β-cell proliferation and reduces apoptosis. These protective effects are largely attributed to various secreted factors, such as secretory proteins and exosomes. Notably, supernatants derived from MSC cultures exhibit effects comparable to those of the MSCs themselves [43]. This study demonstrated that MSC-mediated β-cell protection was dependent on Wnt-mediated extracellular transport. Furthermore, the classical Wnt pathway promoted β-cell proliferation via β-catenin signaling, while the nonclassical Wnt pathway positively regulated insulin secretion by modulating calcium influx. These findings are consistent with prior evidence establishing Wnt signaling as both necessary and sufficient for islet β-cell proliferation, insulin secretion, and tissue inflammation [44–46]. Compromised MSC quality and secretory capacity, especially reduced extracellular Wnt trafficking, are key contributors to β-cell dysfunction and the progression of diabetes from a compensated to a decompensated state.

Immunoregulation is a key characteristic of MSCs, maintaining tissue homeostasis. Given the strong infiltration of pro-inflammatory macrophages and the detrimental effects of TNF-α on β-cell viability observed in diabetes, MSCs may indirectly protect β-cells by promoting macrophage phenotypic switching. In vitro, MSC supplementation reverses the adverse effects of pro-inflammatory macrophages on insulin release from β-cells [42]. Our findings also indicate a cross-regulatory role between MSCs and macrophages, suggesting that these interactions are mutual rather than unidirectional. This reversal is largely dependent on the phenotypic reprogramming of macrophages. The immunomodulatory effects mediated by MSCs are significantly influenced by a robust paracrine component, including PGE2, TSG-6, and Wnt ligands [47]. In

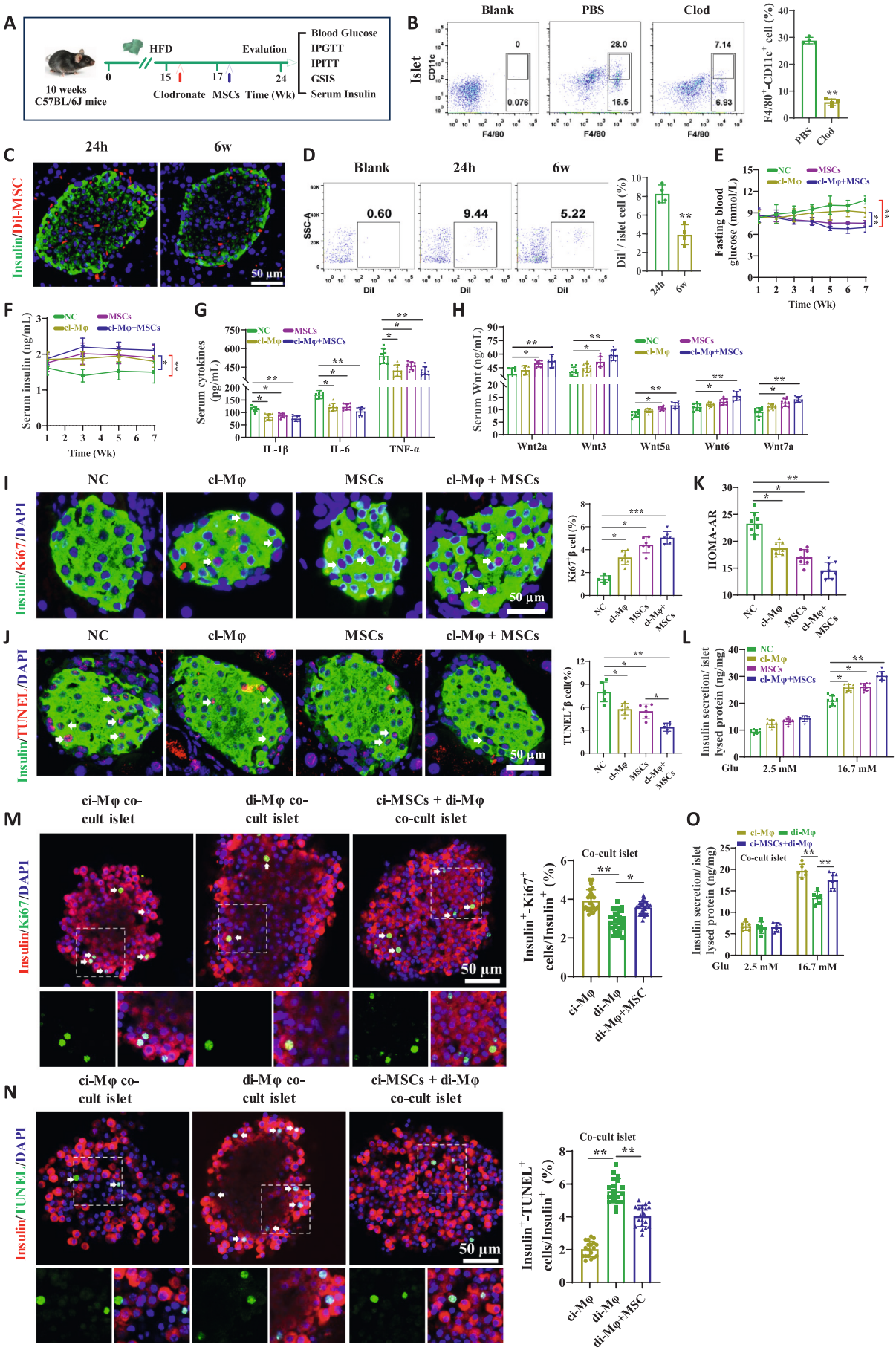

(caption on next page)

Fig. 6. MSC administration combined with macrophage deletion reversing β-cell decompensation. (A) Schematic flowchart of the in vivo experimental design to evaluate the therapeutic effect of MSC injection following macrophage depletion. Ten-week-old C57BL/6J mice were fed a HFD for 15 weeks, then received intraperitoneal clodronate injection (70 μg/g) twice weekly. Two weeks later, 2.5×10^5 MSCs were delivered via pancreatic capsule injection. Multiple physiological indicators were assessed at 6–7 weeks after MSC administration. cl-Mφ: macrophage depletion group; cl-Mφ + MSCs: macrophage depletion plus MSC injection group. (B) Efficiency of macrophage depletion in pancreatic islets after clodronate treatment. Data were analyzed by independent-samples *t*-test ($n = 4$ mice per group); $^{**}p < 0.01$. (C, D) Homing and retention of MSCs in pancreatic islets at 24 h and 6 weeks after pancreatic capsule injection, as determined by fluorescence imaging (C, Scale bar = 50 μm) and flow cytometry (D). Data were analyzed by independent-samples *t*-test (n = 4 mice per group); $^{**}p < 0.01$. (E, F) Fasting blood glucose levels and serum insulin concentrations in mice from each treatment group. Data were analyzed by two-way ANOVA ($n = 8$ mice per group); $^{*}p \leq 0.05$, $^{**}p \leq 0.01$. (G) Serum inflammatory cytokine levels in each treatment group. Data were analyzed by one-way ANOVA (n = 8 mice per group); $^{*}p \leq 0.05$, $^{**}p \leq 0.01$. (H) Serum Wnt levels in mice from each treatment group. Data were analyzed by one-way ANOVA (n = 8 mice per group); $^{*}p \leq 0.05$, $^{**}p \leq 0.01$. (I, J) Representative images of β-cell proliferation (I) and apoptosis (J) of islets from each treatment group (left), and corresponding quantification of $Ki67^{+}Ins^{+}$ cells (right; no fewer than 6 islets per section were included for statistical analysis). Insulin (green), Ki67 or TUNEL (red), DAPI (blue). White arrows mark Ki67- or TUNEL-positive cells. Scale bar = 50 μm. Data were analyzed by one-way ANOVA ($n = 6$ mice per group); $^{*}p \leq 0.05$, $^{***}p \leq 0.001$. (K) HOMA-IR values for each experimental group. Data were analyzed by one-way ANOVA (n = 8 mice per group); $^{*}p \leq 0.05$, $^{**}p \leq 0.01$. (L) Glucose-stimulated insulin secretion of isolated islets at the indicated glucose concentrations in each group. Data were analyzed by one-way ANOVA (n = 8 mice per group); $^{*}p \leq 0.05$, $^{**}p \leq 0.01$. (M, N) β-cell proliferation (M) and apoptosis (N) of islets co-cultured with ci-MSCs or di-Mφ (left), and corresponding quantification of positive cells (right; no fewer than 20 islets per group were used for statistical analysis). Insulin (green), Ki67 or TUNEL (red), DAPI (blue). White arrows indicate Ki67- or TUNEL-positive cells. Scale bar = 50 μm. Data were analyzed by one-way ANOVA; MSCs and Mφ were isolated from 6 individual mice; $^{*}p \leq 0.05$, $^{**}p \leq 0.01$. (O) Insulin secretion of islets co-cultured with di-Mφ, ci-MSCs, or ci-MSCs + di-Mφ at the indicated glucose concentrations. Data were analyzed by one-way ANOVA; MSCs and Mφ were isolated from 6 individual mice per group; $^{**}p \leq 0.01$. (For interpretation of the references to colour in this figure legend, the reader is referred to the web version of this article.)

our study, MSCs isolated from the decompensated phase of diabetes exhibited impaired Wnt secretion. This functional transition of MSCs plays a significant role in the shift from the compensated to the decompensated stage of the disease. The interplay between macrophages and MSCs is essential for diabetes progression, as the dominant influence of one cell type ultimately determines β-cell fate. These consistent correlations between MSC function and their effects on β-cell and macrophage metabolism suggest that MSCs play a vital role in regulating pancreatic immune processes and metabolic homeostasis.

In this study, we report that MSCs and their immunoregulatory effects during β-cell dysfunction are mediated by communication with macrophages. However, there are several limitations. It remains unclear which type of cellular functional alteration initiated the obesity-to-diabetes transition, despite Dr. Yang et al. reporting that β-cell stress was the initial factor for macrophage recruitment to the islets [48], a finding that warrants further investigation. Second, while in vitro studies have convincingly illustrated the interactions between MSCs and macrophages that influence β-cell function, directly dissecting the effects of MSCs on β-cells in vivo presents significant challenges. Further research is essential to comprehensively understand the interplay between MSCs and macrophages across various pathological conditions. Additionally, the specificity of MSC modulation in vivo during diabetes progression needs to be determined using lineage-specific genetic tools.

5. Conclusion

Our findings reveal that the shift from compensation to decompensation involves complex communication among β-cells, macrophages, and MSCs. This communication, particularly through the macrophage-MSC-Wnt axis, mediates the failure of islet β-cell adaptation. We observed that macrophages and MSCs exhibit unique metabolic phenotypes during both compensation and decompensation phases, and their interaction plays a crucial role in the adaptive function of beta cells. Therefore, strategies aimed at modulating this interplay may provide a promising new therapeutic avenue for the treatment of T2DM.

CRediT authorship contribution statement

Jianxing Liu: Writing – original draft, Investigation, Data curation, Conceptualization. **Weilong Xu:** Investigation, Data curation. **Wenjing Yan:** Investigation, Data curation. **Yimeng Qin:** Formal analysis. **Xintong Wang:** Visualization. **Xiuning Chen:** Project administration. **Zhaoyou Meng:** Supervision. **Yi Pan:** Software. **Yanfeng Zhang:** Supervision. **Yumeng Shen:** Validation. **Yue Yang:** Visualization. **Fangfang Zhang:** Project administration. **Hailiang Liu:** Resources. **Pengfei Zheng:** Resources. **Jiangyi Yu:** Funding acquisition. **Liang Jin:** Writing – review & editing, Funding acquisition, Conceptualization.

Funding

This work was supported by the National Natural Science Foundation of China (Grant Nos. 82373925, 82370804, 82374355), the Key Project of Xinjiang Production and Construction Corps Natural Science Fund (2025DA013), and the Open Project of the Carthamus Tinctorius Industry Research Institute of Shihezi University (CZ2024KFG04).

Declaration of competing interest

All authors declare no conflicts of interest with regard to the publication of this paper.

Acknowledgements

We thank the Public Laboratory Platform of China Pharmaceutical University for supporting this work.

Appendix A. Supplementary data

Supplementary data to this article can be found online at https://doi.org/10.1016/j.metabol.2026.156636.

Data availability

All relevant data within this paper are available upon request to the corresponding author.

References

[1] Kubo H, Imai J, Izumi T, et al. Colonic inflammation triggers β cell proliferation during obesity development via a liver-to-pancreas interorgan mechanism. JCI Insight 2025;10:e183864.
[2] Wang RR, Qiu X, Pan R, et al. Dietary intervention preserves beta cell function in mice through CTCF-mediated transcriptional reprogramming. J Exp Med 2022;219:e20211779.
[3] You X, Peng Q, Qian W, et al. SRSF1 is essential for pancreatic beta-cell proliferation and the maintenance of glucose homeostasis in mice. Metabolism 2026;174:156421.
[4] Dos Reis Araujo T, Da Silva Junior JA, Alves BL, et al. Disruption of mitochondria-associated membranes contributes to the dysregulation of insulin secretion in undernutrition, obesity, and double burden of malnutrition. Metabolism 2025;173:156393.
[5] Cai Z, Yang Y, Zhong J, et al. cGAS suppresses beta-cell proliferation by a STING-independent but CEBPbeta-dependent mechanism. Metabolism 2024;157:155933.
[6] Magkos F, Lee MH, Lim M, et al. Dynamic assessment of insulin secretion and insulin resistance in Asians with prediabetes. Metabolism 2022;128:154957.

[7] Holendová B, Šalovská B, Benáková Š, et al. Beyond glucose: the crucial role of redox signaling in β-cell metabolic adaptation. Metabolism 2024;161.
[8] Chen X, Shao J, Brandenburger I, et al. FFAR4-mediated IL-6 release from islet macrophages promotes insulin secretion and is compromised in type-2 diabetes. Nat Commun 2025;16:3422.
[9] Gottmann P, Speckmann T, Stadion M, et al. Transcriptomic heterogeneity of non-beta islet cells is associated with type 2 diabetes development in mouse models. Diabetologia 2024;68:166–85.
[10] Akhtar MN, Hnatiuk A, Delgadillo-Silva L, et al. Developmental beta-cell death orchestrates the islet's inflammatory milieu by regulating immune system crosstalk. EMBO J 2025;44:1131–53.
[11] Jiang Q, Zhao Q, Chen Y, et al. Galectin-3 impairs calcium transients and β-cell function. Nat Commun 2024;15:3682.
[12] Migliorini A, Ge S, Atkins MH, et al. Embryonic macrophages support endocrine commitment during human pancreatic differentiation. Cell Stem Cell 2024;31:1591–611. e8.
[13] Hong Z, Chen S, Sun J, et al. STING signaling in islet macrophages impairs insulin secretion in obesity. Sci China Life Sci 2024;67:345–59.
[14] Cherubini A, Pistoni C, Iachini MC, et al. R-spondins secreted by human pancreas-derived mesenchymal stromal cells support pancreatic organoid proliferation. Cell Mol Life Sci 2025;82:125.
[15] Chen X, An H, Du Y, et al. hucMSC-derived exosomes targeting macrophage polarization attenuate systemic inflammation in T1DM via INS/SOD1 delivery. Stem Cell Res Ther 2025;16:384.
[16] Du F, Liu M, Wang J, et al. Metformin coordinates with mesenchymal cells to promote VEGF-mediated angiogenesis in diabetic wound healing through Akt/mTOR activation. Metabolism 2023;140:155398.
[17] Campa-Carranza JN, Capuani S, Joubert AL, et al. Immune and angiogenic profiling of mesenchymal stem cell functions in a subcutaneous microenvironment for allogeneic islet transplantation. Adv Sci 2025;12:e2411574.
[18] Dadheech N, Srivastava A, Vakani M, et al. Direct lineage tracing reveals Activin-a potential for improved pancreatic homing of bone marrow mesenchymal stem cells and efficient ß-cell regeneration in vivo. Stem Cell Res Ther 2020;11:327.
[19] Khatri R, Petry SF, Linn T. Intrapancreatic MSC transplantation facilitates pancreatic islet regeneration. Stem Cell Res Ther 2021;12:121.
[20] Cooper TT, Sherman SE, Bell GI, et al. Characterization of a Vimentinhigh/Nestinhigh proteome and tissue regenerative secretome generated by human pancreas-derived mesenchymal stromal cells. Stem Cells 2020;38:666–82.
[21] Zang L, Li Y, Hao H, et al. Efficacy and safety of umbilical cord-derived mesenchymal stem cells in Chinese adults with type 2 diabetes: a single-center, double-blinded, randomized, placebo-controlled phase II trial. Stem Cell Res Ther 2022;13:180.
[22] Liu Y, Yang Y, Xu C, et al. Circular RNA circGlis3 protects against islet β-cell dysfunction and apoptosis in obesity. Nat Commun 2023;14:351.
[23] Zhang F, Yang Y, Chen X, et al. The long non-coding RNA βFaar regulates islet β-cell function and survival during obesity in mice. Nat Commun 2021;12:3997.
[24] Kalucka J, De Rooij LPMH, Goveia J, et al. Single-cell transcriptome atlas of murine endothelial cells. Cell 2020;180:764–79. e20.
[25] Zhang FF, Liu YH, Wang DW, et al. Obesity-induced reduced expression of the lncRNA ROIT impairs insulin transcription by downregulation of Nkx6.1 methylation. Diabetologia 2020;63:811–24.
[26] Stangé M V D C Geert, Heimberg Harry. Purification of rat pancreatic B-cells by fluorescence-activated cell sorting. Methods Mol Med 2003;83:15–22.
[27] Wang D, Qin Y, Huang B, et al. Adipocyte microRNA-802 promotes adipose tissue inflammation and insulin resistance by modulating macrophages in obesity. eLife 2024;13:e99162.
[28] Virtue S, Vidal-Puig A. GTTs and ITTs in mice: simple tests, complex answers. Nat Metab 2021;3:883–6.
[29] Weir Gc, B-W S. Five stages of evolving beta-cell dysfunction during progression to diabetes. Diabetes 2004;3:S16–21.
[30] Clevers H, Loh KM, Nusse R. An integral program for tissue renewal and regeneration: Wnt signaling and stem cell control. Science 2014;346:1248012.
[31] Ying W, Lee YS, Dong Y, et al. Expansion of islet-resident macrophages leads to inflammation affecting β cell proliferation and function in obesity. Cell Metab 2019;29:457–74. e5.
[32] Holendova B, Salovska B, Benakova S, et al. Beyond glucose: the crucial role of redox signaling in beta-cell metabolic adaptation. Metabolism 2024;161:156027.
[33] Patel SYZ, Remedi Ms. Intermittent fasting protects β-cell identity and function in a type-2 diabetes model. Metabolism 2024;153:155813.
[34] Chan JY, Lee K, Maxwell EL, et al. Macrophage alterations in islets of obese mice linked to beta cell disruption in diabetes. Diabetologia 2019;62:993–9.
[35] Saunders DC, Aamodt KI, Richardson TM, et al. Coordinated interactions between endothelial cells and macrophages in the islet microenvironment promote β cell regeneration. npj Regen Med 2021;6:22.
[36] Leng S, Zhang X, Zhao R, et al. Mechanical activation of adipose tissue macrophages mediated by Piezo1 protects against diet-induced obesity by regulating sympathetic activity. Metabolism 2025;168.
[37] Varthaliti A, Lygizos V, Fanaki M, et al. The role of IL-6 and TNF-α as early biomarkers in the prediction and diagnosis of gestational diabetes mellitus. Biomedicines 2025;13:1627.
[38] Javaid HMA, Ko E, Joo EJ, et al. TNFα-induced NLRP3 inflammasome mediates adipocyte dysfunction and activates macrophages through adipocyte-derived lipocalin 2. Metabolism 2023;142.
[39] Rogulska O, Vavrinova E, Vackova I, et al. The role of cytokine licensing in shaping the therapeutic potential of wharton's jelly MSCs: metabolic shift towards immunomodulation at the expense of differentiation. Stem Cell Res Ther 2025;16:199.
[40] Zong Q, Bundkirchen K, Neunaber C, et al. Effect of high BMI on human bone marrow–derived mesenchymal stromal cells. Cell Transplant 2024;33:9636897241226546.
[41] Xing S-J, Gao Y-F, Liu L, et al. Integrated phenotypic and transcriptomic analyses of osteoporosis in type 2 diabetic mice. Int J Med Sci 2025;22:1773–90.
[42] Gou W, Hua W, Swaby L, et al. Stem cell therapy improves human islet graft survival in mice via regulation of macrophages. Diabetes 2022;71:2642–55.
[43] Alvaro Moreira RN, Hall Kristen, Emukah Chimobi, Martinez John, Moreira Axel, Dittmar Evan, et al. Effects of mesenchymal stromal cell-conditioned media on measures of lung structure and function a systematic review and meta-analysis of preclinical studies. Stem Cell Res Ther 2020;11:399.
[44] Maschio DA, Hernandes LHP, Alvares LE, et al. Differential expression of regulators of the canonical Wnt pathway during the compensatory beta-cell hyperplasia in prediabetic mice. Biochem Biophys Res Commun 2022;611:183–9.
[45] Chen J, Ning C, Mu J, et al. Role of Wnt signaling pathways in type 2 diabetes mellitus. Mol Cell Biochem 2021;476:2219–32.
[46] Leanza G, Faraj M, Cannata F, et al. Bone inflammation in postmenopausal women with type 2 diabetes or obesity in relation to Wnt signaling and bone strength. Metabolism 2026;177.
[47] Wang Z, Sun Y, Shen R, et al. Global scientific trends on the immunomodulation of mesenchymal stem cells in the 21st century: a bibliometric and visualized analysis. Front Immunol 2022;13:984984.
[48] Yang B, Yang L, Wang Y, et al. Macrophages and neutrophils are necessary for ER stress-induced β cell loss. Cell Rep 2022;40:111255.